Nomoto et al. Nanoscale Research Letters (2016) 11:320
DOI 10.1186/s11671-016-1535-1

Nanoscale Research Letters

NANO EXPRESS Open Access

High-Hall-Mobility Al-Doped ZnO Films Having Textured Polycrystalline Structure with a Well-Defined (0001) Orientation

Junichi Nomoto*, Hisao Makino and Tetsuya Yamamoto

Abstract

Five hundred-nanometer-thick ZnO-based textured polycrystalline films consisting of 490-nm-thick Al-doped ZnO (AZO) films deposited on 10-nm-thick Ga-doped ZnO (GZO) films exhibited a high Hall mobility (μ_H) of 50.1 cm^2/Vs with a carrier concentration (N) of 2.55×10^{20} cm^{-3}. Firstly, the GZO films were prepared on glass substrates by ion plating with dc arc discharge, and the AZO films were then deposited on the GZO films by direct current magnetron sputtering (DC-MS). The GZO interface layers with a preferential c-axis orientation play a critical role in producing AZO films with texture development of a well-defined (0001) orientation, whereas 500-nm-thick AZO films deposited by only DC-MS showed a mixture of the c-plane and the other plane orientation, to exhibit a μ_H of 38.7 cm^2/Vs with an N of 2.22×10^{20} cm^{-3}.

Keywords: Carrier transport, Transparent conducting oxide, X-ray diffraction, Al-doped ZnO, Ga-doped ZnO, Magnetron sputtering, Ion plating

Background

We demonstrate a nanoscale material design to achieve high-Hall-mobility Al-doped ZnO (AZO) textured polycrystalline films with a well-defined (0001) orientation. The key factor is to enhance intragrain carrier mobility together with a substantial reduction of the contribution of grain boundary (GB) scattering to carrier transport due to a high degree of c-axis alignment between columnar grains. AZO films have recently been focused on as an alternative to tin-doped indium oxide (In_2O_3:Sn) and fluorine-doped tin oxide (SnO_2:F) films for use as the transparent electrodes of flat panel displays and in the window layers of solar cells [1–4]. In our previous work [5], we investigated the characteristics of AZO films deposited by direct current magnetron sputtering (DC-MS), radio frequency (RF)-MS, and RF-superimposed DC-MS (RF/DC-MS) with a systematic variation of the power ratio of DC to RF to clarify key factors that determine the carrier transport. We used sintered oxide argets with an Al_2O_3 content of 2.0 wt.%. The AZO films deposited by DC-MS had a high carrier concentration (N), however, showing poor c-axis alignment between the columnar grains of the polycrystalline structure with textures having a mixed orientation of atomically closely packed (0001) and $(10\bar{1}1)$ planes, whereas AZO films with a low N deposited by RF-MS exhibited a texture consisting of well-aligned columnar grains that showed a preferential c-axis orientation perpendicular to the substrate. Analysis of the relationship between the carrier transport and the orientation distribution of AZO films by various MS techniques showed that the presence of the $(10\bar{1}1)$ orientation texture can increase the contribution of GB scattering to carrier transport, resulting in a reduced Hall mobility (μ_H). The above contribution was defined as the ratio of the optical mobility (μ_{opt}) corresponding to intragrain carrier mobility to the carrier mobility at the GBs (μ_{GB}), $\mu_{opt}/\mu_{GB} = (\mu_{opt} - \mu_H)/\mu_H$ [5]. μ_{opt} was calculated on the basis of the Drude theory with the Tauc-Lorentz model [6–10] using optical data such as optical transmittance and reflectance. From those findings, an issue to be resolved to achieve high-μ_H AZO films with low electrical resistivity (ρ) is to develop a deposition technology to realize AZO films with a well-defined single (0001) orientation by DC-MS.

* Correspondence: nomoto.junichi@kochi-tech.ac.jp
Research Institute, Kochi University of Technology, 185 Miyanokuchi, Tosayamada-cho, Kami-shi, Kochi 782-8502, Japan

In this work, on the basis of many reports on controlling the crystallinity and/or surface morphology of AZO films in the early growth stages [11–18], we propose a resolution to the issue; a critical layer (CL) made from 10-nm-thick Ga-doped ZnO (GZO) films with a preferential *c*-axis orientation normal to the substrate as an interface layer between thicker AZO films by DC-MS and substrates. The CL comprises GZO films deposited by ion plating (IP) with dc arc discharge. The IP technique enables us with the optimization of the energy of the incident particles from the target to the substrate surface, with a high plasma density in the order of 10^{12}/cm^3 resulting in high ionization rates of Zn, Ga, and O atoms, to promote the formation of the columnar grains with the highly preferential *c*-axis orientation owing to the well-defined (0001) orientation in the entire GZO films and to enhance high lateral diffusion of the above species leading to the films exhibiting the flat surface [19, 20]. The CLs play a critical role in achieving the AZO films having a textured polycrystalline structure with a well-defined single (0001) orientation.

It also should be noted that for wide applications of highly transparent conducting AZO films, taking into account the fact that N in the range from 4× to 6 × 10^{20} cm^{-3} gives rise to the reduction in the optical transmittance from the visible (VIS) to near-infrared (NIR) wavelength region due to the free carrier absorption, the magnitude of N should be in the range from 2× to 3 × 10^{20} cm^{-3}. In the present work, we, thus, used sintered oxide targets with an Al_2O_3 content of 0.5 wt.%. In such case, high μ_H is essential for use as highly transparent conducting films. We demonstrate that the use of CLs is an effective way to achieve the above films.

We investigated the effects of the improved orientation distribution due to the use of CLs on the electrical and optical properties to clarify a limiting factor of carrier transport of AZO films by DC-MS.

Methods

Film Deposition

We deposited 500-nm-thick AZO films on glass substrates (Corning Eagle XG) or 490-nm-thick AZO films on 10-nm-thick CLs prepared on the glass substrates at a substrate temperature of 200 °C by DC-MS with a power of 200 W. We used an MS apparatus (ULVAC CS-L) to deposit the AZO films [5]. The sintered oxide targets (Toshima Manufacturing Corp.) were high-density sintered circular AZO targets (diameter: 80 mm) with an Al_2O_3 content of 0.5 wt.%. We deposited 10-nm-thick CLs made from GZO films on the glass substrates using IP apparatus (Sumitomo Heavy Industries, Ltd.) with a dc arc discharge current of 150 A. We introduced oxygen (O_2) gas with a flow rate of 10 sccm into the chamber to control the density of oxygen-related point defects such as oxygen vacancies and interstitials in the film. The evaporation source (HAKUSUI Tech. SKY-Z) for the deposition of CLs was sintered ceramic ZnO (99.99 % purity) containing 4.0 wt.% Ga_2O_3 (99.9 % purity) [10, 20].

Characterization

The film thickness was measured using a surface profilometer (KLA Tencor, Alpha-Step IQ). N, μ_H, and ρ were determined by Hall effect measurements (Nanometrics, HL5500PC) at a room temperature using the van der Pauw method. Indium paste was used as an ohmic contact electrode between measuring styluses and surface of AZO films.

The out-of-plane $\theta/2\theta$ X-ray diffraction (XRD) pattern and out-of-plane rocking curve were obtained. For a comprehensive analysis of the texture evolution, we carried out out-of-plane grazing-incidence XRD (GIXRD) measurements, where the X-ray incident beam angle (ω) was fixed at 0.35° and only the 2θ axis was scanned [21–24]. The crystal structure of the films was characterized by out-of-plane wide-range reciprocal space maps (RSMs) obtained using the SmartLab high-resolution XRD system (Rigaku corp.) equipped with a PILATUS 100K/R two-dimensional (2D) X-ray detector using Cu-K $\bar{a}$ (wavelength $\lambda = 0.15418$ nm) radiation [25, 26]. The optical properties were measured using a spectrophotometer (Hitachi, U-4100) and a spectroscopic ellipsometer (SE; J.A. Woollam, M-2000DI). The optical transmittance (T) and reflectance (R) spectra of the ZnO-based films in the wavelength (λ) range from 200 to 2400 nm were obtained using a spectrophotometer with an incident angle of light of 5°. The ellipsometric data (Ψ and Δ) [10] were acquired in the wavelength range from 300 to 1700 nm at incident angles of 55° to 75° in 5° step.

Results and Discussion

Figure 1(a) shows out-of-plane $\theta/2\theta$ XRD patterns for AZO films without and with CLs. The analysis of the out-of-plane $\theta/2\theta$ XRD patterns of the two different types of AZO films shows that the intensity of wurtzite ZnO 0002 peak is much higher than those of the other peaks. For AZO films without CLs, several peaks except for the 0002 peak were clearly observed. The out-of-plane $\theta/2\theta$ XRD patterns of AZO films without CLs in the 2θ ranges from 40° to 80° and from 80° to 120° are shown in Fig. 1(b, c), respectively: the peaks of the $10\bar{1}1$, $10\bar{1}2$, $10\bar{1}3$, $10\bar{1}5$, $11\bar{2}0$, $11\bar{2}2$, $20\bar{2}1$, $20\bar{2}2$, and $30\bar{3}2$ reflections together with those of the 0002, 0004, and 0006 reflections were observed. On the other hand, for AZO films with CLs, we found high intensities of the 0002, 0004, and 0006 reflections compared with those of the CL-free AZO films. Note that unlike CL-free AZO

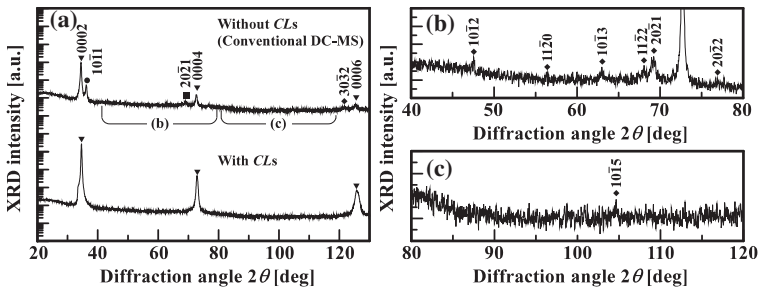

Fig. 1 Out-of-plane $\theta/2\theta$ XRD patterns of AZO films (**a**) without and with CLs and of CL-free AZO films in the 2θ ranges (**b**) from 40° to 80° and (**c**) from 80° to 120°

films, as shown in Fig. 1(a), no other peaks have been observed for AZO films with CLs, as shown in Fig. 1(b, c).

To investigate what causes the significant difference in the above behavior of the reflections, as shown in Fig. 1(a–c), between AZO films with and without CLs, we examined the location of the center of gravity of the diffraction peaks obtained by wide-range RSMs. Figure 2 shows the following results: $q_{//}$ and $q_{\perp}$ represent the coordinates of the reciprocal space ($q = 1/d_{hkil} = 2\sin\theta/\lambda$, θ and λ are the incident angle and the wavelength of the X-rays, respectively); $q_{//}$ is parallel to the surface, and $q_{\perp}$ is perpendicular to the surface. The solid and long-dashed directional lines correspond to orbitals for the out-of-plane $\theta/2\theta$ XRD and GIXRD scans, respectively. For the AZO films without CLs, as shown in Fig. 2a, the analysis of the data obtained by RSMs showed the peaks of the $10\bar{1}1$, $10\bar{1}2$, $10\bar{1}3$, $10\bar{1}5$, $11\bar{2}0$, $11\bar{2}2$, $20\bar{2}1$, $20\bar{2}2$, and $30\bar{3}2$ reflections together with those of the 0002, 0004, and 0006 reflections. Note that the center of gravity of the peaks of the symmetrical $10\bar{1}1$, $20\bar{2}1$, $20\bar{2}2$, and $30\bar{3}2$ reflections was observed to be located approximately on a vertical line in the RSMs. In addition, the center of gravity of the peaks of the other reflections such as $10\bar{1}2$, $10\bar{1}3$, $10\bar{1}5$, $11\bar{2}0$, and $11\bar{2}2$ reflections were located on an asymmetrical zones in RSMs. This proves that the $(10\bar{1}1)$, $(20\bar{2}1)$, and $(30\bar{3}2)$ planes of the AZO films without CLs lie approximately parallel to a substrate surface. On the other hand, the polycrystalline AZO films with CLs, as shown in Fig. 2b, show a distinct feature: we found that only {0001} family of planes was parallel to the substrate surface. This indicates that the AZO films with CLs exhibit a high degree of *c*-axis alignment between columnar grains: we confirmed a small full width at half maximum of the ω rocking curves (FWHMω) for the 0002 peak of 1.81° compared with those, FWHMω >2, for GZO films deposited by IP with dc arc discharge in our previous work [10].

Next, we investigated the effects of CLs on the electrical properties of AZO films with CLs. Table 1 summarizes the results of Hall effect measurements at a room temperature. In this study, taking into account the fact that the thickness of CLs was 10 nm, which was very thin compared with the total thickness of the samples of 500 nm, the discussion below is based on a single-layer model. We obtained the following results in

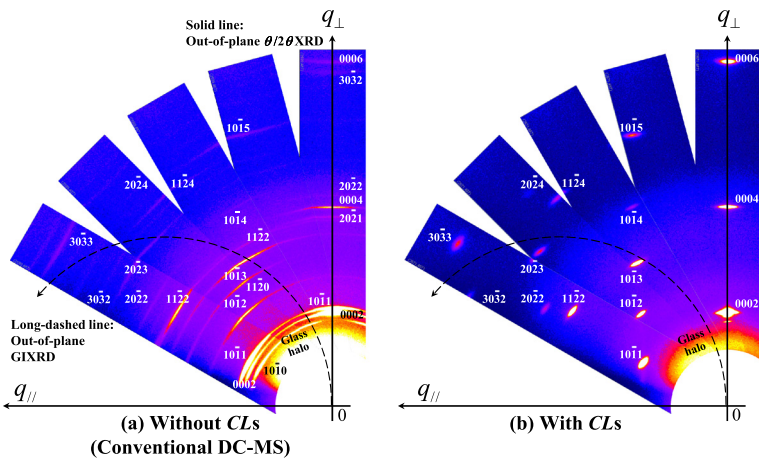

Fig. 2 Wide-range reciprocal space maps (RSMs) of 500-nm-thick AZO films **a** without and **b** with CLs

Table 1 Electrical resistivity (ρ), carrier concentration (N), Hall mobility (μ_H), optical mobility (μ_{opt}), the contribution of grain boundary scattering to carrier transport (μ_{opt}/μ_{GB}; carrier mobility at grain boundaries), effective mass of electrons (m^*), plasma frequency (ω_p), and high-frequency dielectric constant (ε_∞) of AZO films with and without CLs

Structure	ρ (Ωcm)	N (cm^{-3})	μ_H (cm^2/Vs)	μ_{opt} (cm^2/Vs)	μ_{opt}/μ_{GB}	m^*	ω_p (rad/s)	ε_∞
With CLs	4.89×10^{-4}	2.55×10^{20}	50.1	50.1	0.00	0.24	9.32×10^{14}	3.96
Without CLs	7.26×10^{-4}	2.22×10^{20}	38.7	51.1	0.32	0.23	8.83×10^{14}	3.92

the experiments: the AZO films with CLs showed a lower ρ of 4.89×10^{-4} Ωcm with a μ_H of 50.1 cm^2/Vs and an N of 2.55×10^{20} cm^{-3}, whereas CL-free AZO films exhibited a higher ρ of 7.26×10^{-4} Ωcm with a μ_H of 38.7 cm^2/Vs and an N of 2.22×10^{20} cm^{-3}. The cause of the drastic reduction in ρ of the AZO films with CLs compared with that of the CL-free AZO films is an enhancement in both μ_H and N, considering the inversely proportional relationship between ρ and the product of μ_H and N. The use of CLs produced a distinct increase in μ_H for AZO films by 29 % together with an increase in N by 15 %. Several investigations on the control of μ_H for almost same values of N have been conducted for the following films: (1) ZnO films codoped with Al and hydrogen deposited by RF-MS [27], (2) AZO films deposited by RF-MS [28] and DC reactive MS [29], and (3) boron (B)-doped ZnO (BZO) deposited by pulsed laser deposition (PLD) [30]. In general, the growth temperature, thickness, and types of the substrates strongly affect the electrical properties of AZO films regardless of the deposition methods. Therefore, we compare the films deposited in this study with 500-nm-thick BZO films deposited on a glass substrate at a temperature of 200 °C by PLD, for which μ_H and N were reported to be 47.2 cm^2/Vs and 2.97×10^{20} cm^{-3}, respectively [30]. Considering that the MS and IP techniques have the advantages of growth areas and deposition rates over the PLD technique, the use of nanometer-thick CLs with these deposition methods is very effective for achieving high-μ_H AZO films not only from academic nanoengineering research but also from industrial engineering viewpoints.

In the following, to obtain a better understanding of the change in μ_H attributed to the use of the CLs, we calculated μ_{opt}/μ_{GB} on the basis of Matthiessen's rule, $(\mu_H)^{-1} = (\mu_{opt})^{-1} + (\mu_{GB})^{-1}$ [5]. μ_{opt} was calculated on the basis of the Drude theory [5–10] using the experimental data for Ψ and Δ determined by spectroscopic ellipsometry measurements combined with experimental data for T and R determined by spectrophotometer measurements. To describe the optical response due to free electrons, the dielectric function of AZO films based on the conventional Drude model (ε_D) is expressed by

$$\varepsilon_D(E) = -\frac{A_D}{E^2 - i\Gamma_D E}, \tag{1}$$

where A_D and Γ_D are the oscillator amplitude and broadening parameter, respectively [5–10]. In the Drude theory for free electrons, Γ_D is expressed as

$$\Gamma_D = \frac{\hbar e}{m^* \mu_{opt}}, \tag{2}$$

where $\hbar \equiv h/2\pi$ (h is Planck's constant), e is the electron charge, and m^* is the effective mass of electrons. In this study, we calculated m^* by the following process. In the Drude model, the real part of ε_D ($Re\varepsilon_D$) is given by

$$Re\varepsilon_D = \varepsilon_D' = n^2 - k^2 = \varepsilon_\infty \left(1 - \frac{\omega_p^2}{\omega^2 + \omega_c^2}\right), \tag{3}$$

where n and k are the refractive index and extinction coefficient, respectively, and ε_∞ is the high-frequency dielectric permittivity due to the bound electrons. In metal-like materials, two characteristic frequencies, the plasma frequency ω_p and collision frequency ω_c, are completely defined by the free carriers; ω_p is given by $\omega_p = ((e^2N)/(m^*\varepsilon_\infty\varepsilon_o))^{1/2}$, where ε_o is the free-space dielectric constant and ω_c is the reciprocal of the relaxation time. In the high-frequency region, where ω_c in Eq. (3) can be neglected, $\varepsilon_D' = \varepsilon_\infty \times (1 - (\omega_p/\omega)^2)$ can be used as a first approximation. By plotting ε_D' versus ω^2, ω_p and ε_∞ can be determined from the gradient and intercept obtained, respectively. Using these values, m^* is calculated from the above expression for ω_p.

Table 1 shows the values of ω_p, ε_∞, and m^* obtained by the best fit in the wavelength range from 0.65 to 0.9 μm. μ_{opt} calculated using Eq. (2) with Γ_D obtained by the SE analysis, calculated values of $m^*$and μ_{opt}/μ_{GB} obtained using Matthiessen's rule with μ_H determined by Hall effect measurements and also tabulated in Table 1. Note that the AZO films with CLs had a μ_{opt} of 50.1 cm^2/Vs together with a μ_{opt}/μ_{GB} of practically zero, leading to no reduction in μ_H to 50.1 cm^2/Vs as a result, whereas the CL-free AZO films had a μ_{opt} of 51.1 cm^2/Vs similar to that of the AZO films with CLs, and, however, exhibited a large μ_{opt}/μ_{GB} of 0.32, resulting in a substantially reduced μ_H of 38.7 cm^2/Vs compared with the above μ_{opt}. This clearly demonstrated that the texture of a

mixture with the (0001) and the other orientations, as shown in Fig. 1(a), gives rise to an increase in the contribution of GB scattering to carrier transport. The CLs play a critical role in substantially reducing the contribution of GB scattering to carrier transport owing to the improved degree of *c*-axis alignment between columnar grains, thereby improving μ_H.

Then, the evolution of the orientation distribution in the initial stage of film growth should be discussed. Figure 3a shows the out-of-plane GIXRD patterns of 10-nm-thick AZO films deposited on glass substrates by DC-MS or CLs, i.e., 10-nm-thick GZO films deposited on glass substrates by IP with dc arc discharge. Figure 3b shows the out-of-plane GIXRD patterns of 50-nm-thick AZO films deposited on glass substrates by DC-MS and 50-nm-thick GZO films deposited on glass substrates by IP with dc arc discharge. The analysis of the out-of-plane GIXRD patterns [21–24] for two different types of ZnO-based films with a thickness of 10 nm in Fig. 3a shows the following: the DC-MS technique produced films with predominant 0002 and $10\bar{1}3$ peaks, whereas the IP technique generated films showing a $10\bar{1}3$ peak with very high intensity and a 0002 peak with very low intensity, which suggests a well-defined (0001) orientation. Upon increasing the thickness to 50 nm (Fig. 3b), the AZO films deposited by DC-MS clearly exhibited the $10\bar{1}0$, $10\bar{1}1$, $10\bar{1}2$, $11\bar{2}0$, and $11\bar{2}2$ peaks in addition to the 0002 and $10\bar{1}3$ peaks. From Figs. 1(b), 2a, and 3b, it is likely that 10-nm-thick AZO films by DC-MS have a polycrystalline textured structure consisting of some crystallites with a low probability of different orientations from the (0001) orientation. On the other hand, Fig. 3a, b shows that the reflections remained the same, corresponding to the 0002 and $10\bar{1}3$ peaks, for the GZO films with different thicknesses prepared by IP with dc arc discharge. This proves that 10-nm-thick GZO films deposited by IP with dc arc discharge show high crystallinity owing to the well-defined (0001) orientation mentioned above over the entire film.

Figure 4 shows a cross-sectional bright-field TEM image of a 10-nm-thick GZO film deposited on glass substrates grown by IP with dc arc discharge. Note that lattice fringes were clearly observed for the film. Qualitative analysis of the data obtained by X-ray reflectivity (XRR) measurements by computer simulation suggests the presence of a multilayer; a GZO film with a higher density/an interfacial about 2-nm-thick GZO layer with a lower density directly/the glass substrate. This implies that ZnO deposition is less favorable at the glass substrate surface, hindering the growth of ZnO-based film for the first few layers. The GZO film can be thinner than expected as a result. The GZO films might relax the misfit by distorting their lattice in the interfacial layer. Consequently, the remaining GZO films with a higher density exhibit the (0001) orientation distribution. The XRR-based study on the dependence of the microstructure on the deposition parameters for very thin ZnO films deposited on glass substrates will be reported elsewhere. From the above findings, the use of high crystal quality CLs exhibiting the

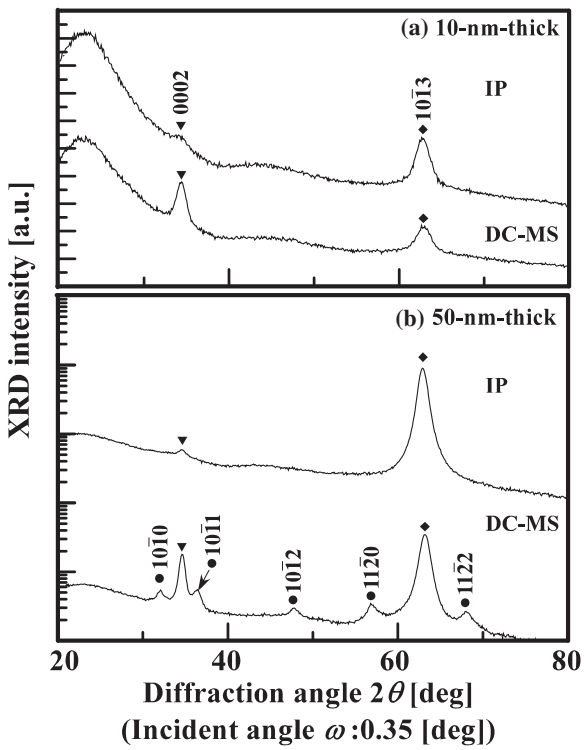

Fig. 3 Out-of-plane GIXRD patterns of **a** 10- and **b** 50-nm-thick AZO films deposited by DC-MS and GZO films prepared by IP with dc arc discharge

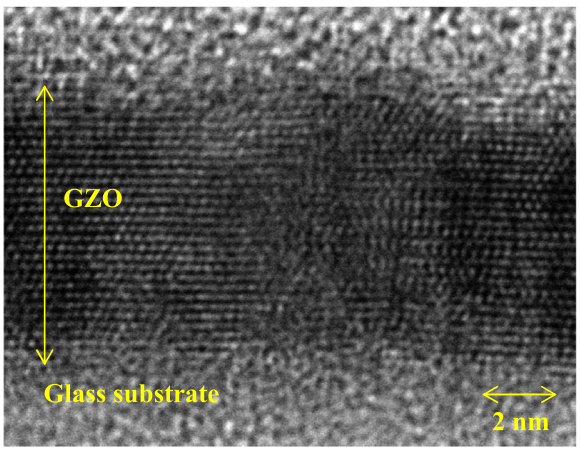

Fig. 4 Cross-sectional bright-field TEM image of a 10-nm-thick GZO film deposited on a glass substrate grown by IP with dc arc discharge

distinct feature of the evolution of the orientation distribution produces AZO polycrystalline films having a textured structure with a well-defined (0001) orientation subsequently grown on the CLs.

Next, we demonstrate the variations in T, R, and absorption coefficient (α) of the AZO films without and with CLs. Figure 5a, b shows the T, R, and α of glass substrates with the two different types of AZO films as functions of wavelength (λ), respectively. α is evaluated using the relation [31, 32]

$$\alpha = \frac{1}{t}\ln\left(\frac{1-R}{T}\right), \tag{4}$$

where t is the film thickness of 500 nm. The α curve of AZO films with CLs in Fig. 5b exhibits a typical characteristic of transparent conductive films, showing the minimum (α_{min}) in the VIS region ranging from 400 to 700 nm. The magnitude of α_{min} would be limited by the absorption mode from various scattering centers such as ionized donor and acceptor impurities, neutral impurities, phonons, and free carriers. Figure 5b clearly demonstrated that the CLs play an important role in substantially reducing α in the VIS region. Considering that the optical absorption in the VIS range is proportional to the number of free carriers and AZO films with CLs had slightly higher N than CL-free AZO films as shown in Table 1, this indicates that, besides free carriers, the other scattering centers, such as n-type oxygen vacancies (V_O) and/or n-type zinc interstitials (Zn_i) and structural defects may also be possibly influencing the absorption source. In our previous work [33], we demonstrated that Ga doping of ZnO films, which leads to an increase in the magnitude of the Madelung energy, enhances the stability of oxygen species in the vicinity of the sites of Ga atoms substituting Zn atoms; some amount of Ga species added to ZnO films removes the ionized point defects such as V_O and/or Zn_i by substituting Zn atoms together with strong attractive Coulomb interaction with the O atoms close to the Ga donors and/or by the reaction with Zn_i thorough repulsive Coulomb interaction between the two different kinds of donors. The two-step deposition process using CLs made from the GZO films can be an effective way to produce AZO films with not only the enhanced preferential c-axis orientation but also improved crystallinity as well as the CLs. The reduction of the above scattering centers consisting of the n-type intrinsic defects would lead to the reduction of optical absorption of AZO films. The behavior of lowered α in the VIS range of AZO films with CLs was observed as a result. In addition, we found that the average T (T_{av}) values in the VIS region of the AZO films without and with CLs were 81.7 and 82.5 %, respectively, as shown in Fig. 5a; the use of CLs causes a slightly increase in T_{av} owing to the improved degree of crystallinity. Figure 5b shows that as λ is increased towards NIR spectral range from 800 to 2400 nm, AZO films with CLs had high α values compared with those of AZO films without CLs at any given λ. This indicates the consistency between α and N of AZO films; the optical absorption in the above spectral range gets influenced by absorption centers, free carriers.

Finally, it should be noted that the CL technique is also very effective for achieving high μ_H AZO films with thinner films as a result of a successful texture-controlled growth: 200- and 100-nm-thick AZO films with the 10-nm-thick CLs show a ρ of 6.91×10^{-4} Ωcm with an N of 2.25×10^{20} cm^{-3} and a μ_H of 40.2 cm^2/Vs and a ρ of 8.34×10^{-4} Ωcm with an N of 2.31×10^{20} cm^{-3} and a μ_H of 32.5 cm^2/Vs, respectively. On the other hand, 200- and 100-nm-thick AZO films without CLs exhibit a ρ of 1.18×10^{-3} Ωcm with an N of 1.82×10^{20} cm^{-3} and a μ_H of 29.2 cm^2/Vs and a ρ of 1.33×10^{-3} Ωcm with an N of 1.75×10^{20} cm^{-3} and a μ_H of 26.9 cm^2/Vs, respectively. These results show that the use of CLs for 200- and 100-nm-thick AZO films enhances N by 23.7 % together with the improvement of μ_H by 37.7 % and increases N by 32.0 % together with the improved μ_H by 20.8 %, resulting in a large decrease in ρ by 41.2 % and by 37.3 % compared with those for 200- and 100-nm-thick AZO films deposited by a conventional DC-MS, respectively. These findings suggest that the development of the CL technique

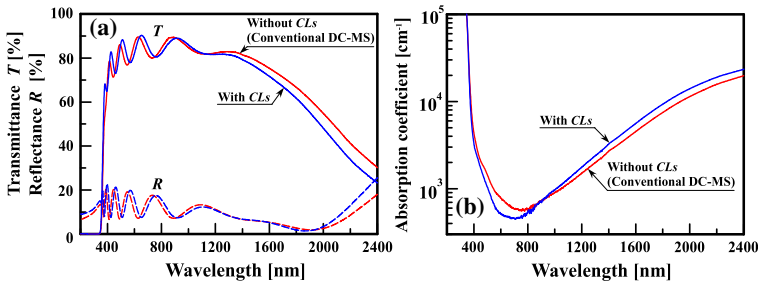

Fig. 5 **a** Optical transmittance (T) and reflectance (R) spectra and **b** absorption coefficient (α) spectra of 500-nm-thick AZO films without and with CLs

is expected to help understand the mechanisms limiting carrier transport of highly doped ZnO polycrystalline films. More study on the effects that the two-step deposition processes using CLs exert on the textured structure and properties of ZnO-based transparent conductive films as a function of total film thickness of less than 500 nm will be given elsewhere.

Conclusions

In this letter, we have reported the development of a two-step deposition process: (1) 10-nm-thick CLs made from GZO films on glass substrates by IP with dc arc discharge and (2) subsequent deposition of 490-nm-thick AZO films on the CLs by DC-MS. This growth method at a substrate temperature of 200 °C was employed to produce AZO films exhibiting high μ_H. The CLs having a texture in which the *c*-axis was preferentially oriented perpendicular to the substrate surface play a critical role in achieving AZO polycrystalline films having a textured structure with a well-defined single (0001) orientation. We have obtained the following experimental results: (1) a small FWHM of the ω rocking curves for the 0002 peak of 1.81°; (2) a high μ_H of 50.1 cm^2/Vs with an N of 2.55×10^{20} cm^{-3}, leading to a low ρ of 4.89×10^{-4} Ωcm. This study clearly shows that a technology to produce AZO films with a high degree of *c*-axis alignment between columnar grains is essential for enhancing intragrain carrier mobility together with little contribution of GB scattering to carrier transport. The development of the CL technique with a nanoscale materials design of very thin films is expected to help us understand the mechanisms of carrier transport of highly doped ZnO polycrystalline films.

Abbreviations

AZO, Al-doped ZnO; BZO, B-doped ZnO; CL, critical layer; dc, direct current; FWHM, full width at half maximum; GB, grain boundary; GIXRD, grazing-incidence x-ray diffraction; GZO, Ga-doped ZnO; IP, ion plating; MS, magnetron sputtering; NIR, near-infrared; PLD, pulsed laser deposition; RF, radio frequency; RSM, reciprocal space maps; VIS, visible; XRD, x-ray diffraction

Competing interests

The authors declare that they have no competing interests.

Authors' contributions

JN has made substantial contributions to the conception of the critical layer, sample fabrication, and data analysis with interpretation, moreover, was involved in drafting and revising the manuscript. MH had made substantial contributions to the sample analysis and discussion about experimental data obtained. TY initiated the idea of working on the present topic and manuscript editing. All authors read and approved the final manuscript.

Acknowledgements

This work was supported by the Japan Society for the Promotion of Science, a Grant-in-Aid for Young Scientists (B) with the title "The control technology and influence of the structural properties of carrier transport for impurity-doped ZnO films" (KAKENHI Grant Number 26790050), and a Basic Research Grant-in-Aid (A) with the title "High- performance ZnO-based hydrogen gas sensor" (KAKENHI Grant Number 30320120).

Received: 28 March 2016 Accepted: 24 June 2016
Published online: 30 June 2016

References

1. Minami T (2000) New n-type transparent conducting oxides. MRS Bull 25:38–44
2. Kushiya K, Kuriyama S, Hara I, Nagoya Y, Tachiyuki M, Fujiwara Y (2002) Progress in large-area CIGS-based modules with sputtered-GZO window. In: Proceedings of 29th IEEE Photovoltaic Specialists Conference, Institute of Electrical and Electronics Engineers, New Orleans, LA, p 579–582
3. Yamamoto T, Yamada T, Miyake A, Makino H, Yamamoto N (2008) Ga-doped zinc oxide: an attractive potential substitute for ITO, large area coating, and control of electrical and optical properties on glass and polymer substrates. J Soc Inf Display 16(7):713–719
4. Yamamoto N, Makino H, Osone S, Ujihara A, Ito T, Hokari H, Maruyama T, Yamamoto T (2012) Development of Ga-doped ZnO transparent electrodes for liquid crystal display panels. Thin Solid Films 520:4131–4138
5. Nomoto J, Makino H, Yamamoto T (2015) Carrier mobility of highly transparent conductive Al-doped ZnO polycrystalline films deposited by radio-frequency, direct-current, and radio-frequency-superimposed direct-current magnetron sputtering: grain boundary effect and scattering in the grain bulk. J Appl Phys 117:045304-1-9
6. Fujiwara H, Kondo M (2005) Effects of carrier concentration on the dielectric function of ZnO:Ga and In_2O_3 :Sn studied by spectroscopic ellipsometry: analysis of free-carrier and band-edge absorption. Phys Rev B 71:075109-1-10
7. Steinhauser J, Faÿ S, Oliveira N, Vallat-Sauvain E, Ballif C (2007) Transition between grain boundary and intragrain scattering transport mechanisms in boron-doped zinc oxide thin films. Appl Phys Lett 90:42107-1-3
8. Volintiru I, Creatore M, van de Sanden MCM (2008) In situ spectroscopic ellipsometry growth studies on the Al-doped ZnO films deposited by remote plasma-enhanced metalorganic chemical vapor deposition. J Appl Phys 103:033704-1-10
9. Makino H, Yamamoto N, Miyake A, Yamada T, Hirashima Y, Iwaoka H, Itoh T, Hokari H, Aoki H, Yamamoto T (2009) Influence of thermal annealing on electrical and optical properties of Ga-doped ZnO thin films. Thin Solid Films 518:1386–1389
10. Yamada T, Makino H, Yamamoto N, Yamamoto T (2010) Ingrain and grain boundary scattering effects on electron mobility of transparent conducting polycrystalline Ga-doped ZnO films. J Appl Phys 107:123534-1-8
11. Sommer N, Stanley M, Köhler F, Mock J, Hüpkes J (2015) Role of the dopant aluminum for the growth of sputtered ZnO:Al investigated by means of a seed layer concept. J Appl Phys 118:035301-1-10
12. Tseng HC, Wang HW, Chang CH, Chou PC, Hsu YC (2010) Effects of sputtering pressure and Al buffer layer thickness on properties of AZO films grown by rf magnetron sputtering. Vacuum 85:263–267
13. Shi HJ, Huang MS, Chu BJ, Zhu BH, Wang AZ, Li DX, Zhang WD, Sun Z, Cheng JW, Huang QF, Yin JX (2010) Effect of ZnO buffer layer on AZO film properties and photovoltaic applications. J Mater Sci Mater Electron 21: 1005–1013
14. Moon T, Yoon W, Ji SK, Ahn WS, Lee S, Joo M, Shin YH, Park K, Lee MH (2010) Microstructure and light-scattering properties of ZnO:Al films prepared using a two-step process through the control of oxygen pressure. Appl Phys Express 3:095801-1-3
15. Nomoto J, Oda J, Miyata T, Minami T (2010) Effect of inserting a buffer layer on the characteristics of transparent conducting impurity-doped ZnO thin films prepared by dc magnetron sputtering. Thin Solid Films 519:1587–1593
16. Itagaki N, Kuwahara K, Nakahara K, Yamashita D, Uchida G, Koda K, Shiratani M (2011) Highly conducting and very thin ZnO:Al films with ZnO buffer layer fabricated by solid phase crystallization from amorphous phase. Appl Phys Express 4:011101-1-3
17. Dewald W, Sittinger V, Szyszka B, Säuberlich F, Stannowski B, Köhl D, Ries P, Wuttig M (2013) Advanced properties of Al-doped ZnO films with a seed layer approach for industrial thin film photovoltaic application. Thin Solid Films 534:474–481
18. Kusayanagi M, Uchida A, Oka N, Jia J, Nakamura S, Shigesato Y (2014) Al-doped ZnO films deposited on a slightly reduced buffer layer by reactive dc unbalanced magnetron sputtering. Thin Solid Films 555:93–99
19. Kitami H, Miyashita M, Sakemi T, Aoki Y, Kato T (2015) Quantitative analysis of ionization rates of depositing particles in reactive plasma deposition using mass-energy analyzer and Langmuir probe. Jpn J Appl Phys 54:01AB05-1-5

20. Nomoto J, Makino H, Yamamoto T (2016) Limiting factors of carrier concentration and transport of polycrystalline Ga-doped ZnO films deposited by ion plating with dc arc discharge. Thin Solid Films 601:13–17
21. Als-Nielsen J, Jacquemain D, Kjaer K, Leveiller F, Lahav M, Leiserowitz L (1994) Principles and applications of grazing incidence X-ray and neutron scattering from ordered molecular monolayers at the air-water interface. Phys Reports 246:251–313
22. Birkholz M (2006) Chaps. 4: Grazing incidence configurations. In: Birkholz M, Fewster PF, Genzel C (eds) Thin film analysis by x-ray scattering. Wiley-VCH Verlag GmbH & Co. KGaA, Weinheim, pp 143–182
23. Birkholz M (2010) A thin film approach to protein crystallography. Nucl Instr Meth B 268:414–419
24. Simeone D, Baldinozzi G, Gosset D, Caer LS, Bérar J-F (2013) Grazing incidence X-ray diffraction for the study of polycrystalline layers. Thin Solid Films 530:9–13
25. Kobayashi S, Inaba K (2012) X-ray thin-film measurement techniques VIII. Detectors and series summary. Rigaku Journal 28(1):8–13
26. Inaba K, Kobayashi S, Uehara K, Okada A, Reddy LS, Endo T (2013) High resolution x-ray diffraction analyses of (La, Sr)MnO3/ZnO/sapphire(0001) double heteroepitaxial films. Adv Mater Phys Chem 3:72–89
27. Duenow NJ, Gessert AT, Wood MD, Young LD, Coutts JT (2008) Effects of hydrogen content in sputtering ambient on ZnO:Al electrical properties. J Non-Cryst Solids 354:2787–2790
28. Berginski M, Hüpkes J, Schulte M, Schöpe G, Stiebig H, Rech B, Wuttig M (2007) The effect of front ZnO:Al surface texture and optical transparency on efficient light trapping in silicon thin-film solar cells. J Appl Phys 101:074903-1-11
29. Jäger S, Szyszka B, Szczyrbowski J, Bräuer G (1998) Comparsion of transparent conductive oxide thin films prepared by a.c. and d.c. reactive magnetron sputtering. Surf Coatings Technol 98:1304–1314
30. Nomoto J, Nishi Y, Miyata T, Minami T (2013) Influence of the kind and content of doped impurities on impurity-doped ZnO transparent electrode applications in thin-film solar cells. Thin Solid Films 534:426–431
31. Kim I, Lee SK, Lee ST, Jeong HJ, Cheong KB, Balk JY, Kim MW (2006) Effect of fluorine addition on transparent and conducting Al doped ZnO films. J Appl Phys 100:063701-1-6
32. Hishikawa Y, Nakamura N, Tsuda S, Nakano S, Kishi Y, Kuwano Y (1991) Interference-free determination of the optical absorption coefficient and the optical gap of amorphous silicon thin films. Jpn J Appl Phys 30:1008–1014
33. Yamamoto T, Katayama-Yoshida H (1999) Solution using a codoping method to unipolarity for the fabrication of p-type ZnO. Jpn J Appl Phys 38(2):L166–L169